Acousto-optic resonant coupling of three spatial modes in an optical fiber

Hee Su Park[1,3] **and Kwang Yong Song**[2,*]

[1]*Korea Research Institute of Standards and Science, Daejeon 305-340, South Korea*
[2]*Department of Physics, Chung-Ang University, Seoul 156-756, South Korea*
[3]*hspark@kriss.re.kr*
[*]*songky@cau.ac.kr*

Abstract: A fiber-optic analogue to an externally driven three-level quantum state is demonstrated by acousto-optic coupling of the spatial modes in a few-mode fiber. Under the condition analogous to electromagnetically induced transparency, a narrow-bandwidth transmission within an absorption band for the fundamental mode is demonstrated. The presented structure is an efficient converter between the fundamental mode and the higher-order modes that cannot be easily addressed by previous techniques, therefore can play a significant role in the next-generation space-division multiplexing communications as an arbitrarily mode-selectable router.

OCIS codes: (060.2340) Fiber optics components; (230.1040) Acousto-optical devices; (270.1670) Coherent optical effects.

References and links

1. S. Longhi, "Quantum-optical analogies using photonic structures," Laser Photonics Rev. **3**, 243–261 (2009).
2. D. Dragoman and M. Dragoman, *Quantum-Classical Analogies* (Springer, Berlin, 2004).
3. C. Ciret, M. Alonzo, V. Coda, A. A. Rangelov, and G. Montemezzani, "Analog to electromagnetically induced transparency and Autler-Townes effect demonstrated with photoinduced coupled waveguides," Phys. Rev. A **88**, 013840 (2013).
4. A. Naweed, G. Farca, S. I. Shopova, and A. T. Rosenberger, "Induced transparency and absorption in coupled whispering-gallery microresonators," Phys. Rev. A **71**, 043804 (2005).
5. Q. Xu, S. Sandhu, M. L. Povinelli, J. Shakya, S. Fan, and M. Lipson, "Experimental realization of an on-chip all-optical analogue to electromagnetically induced transparency," Phys. Rev. Lett. **96**, 123901 (2006).
6. M. F. Yanik, W. Suh, Z. Wang, and S. Fan, "Stopping light in a waveguide with an all-optical analog of electromagnetically induced transparency," Phys. Rev. Lett. **93**, 233903 (2004).
7. L. Maleki, A. B. Matsko, A. A. Savchenkov, and V. S. Ilchenko, "Tunable delay line with interacting whispering-gallery-mode resonators," Opt. Lett. **29**, 626–628 (2004).
8. E. Paspalakis, "Adiabatic three-waveguide directional coupler," Opt. Commun. **258**, 30–34 (2006).
9. S.-Y. Tseng and M.-C. Wu, "Mode conversion/splitting by optical analogy of multistate stimulated Raman adiabatic passage in multimode waveguides," J. Lightwave Technol. **28**, 3529–3534 (2010).
10. X. Xiong, C.-L. Zou, X.-F. Ren, and G.-C. Guo, "Integrated polarization rotator/converter by stimulated Raman adiabatic passage," Opt. Express **21**, 17097–17107 (2013).
11. H. Suchowski, G. Porat, and A. Arie, "Adiabatic processes in frequency conversion," Laser Photonics Rev., doi:10.1002/lpor.201300107 (2013).
12. K. T. McCusker, Y.-P. Huang, A. S. Kowligy, and P. Kumar, "Experimental demonstration of interaction-free all-optical switching via the quantum Zeno effect," Phys. Rev. Lett. **110**, 240403 (2013).
13. D. J. Richardson, J. M. Fini, and L. E. Nelson, "Space-division multiplexing in optical fibres," Nat. Photonics **7**, 354–362 (2013).
14. N. Bozinovic, Y. Yue, Y. Ren, M. Tur, P. Kristensen, H. Huang, A. E. Willner, and S. Ramachandran, "Terabit-scale orbital angular momentum mode division multiplexing in fibers," Science **340**, 1545–1548 (2013).
15. H. S. Park, K. Y. Song, S. H. Yun, and B. Y. Kim, "All-fiber wavelength-tunable acoustooptic switches based on intermodal coupling in fibers," J. Lightwave Technol. **20**, 1864–1868 (2002).

#202694 - $15.00 USD Received 6 Dec 2013; revised 10 Jan 2014; accepted 12 Jan 2014; published 23 Jan 2014

16. The indices i and j of a linearly polarized LP_{ij} mode denote the number of asymmetry axes and the number of lobes along the radius, respectively, of the transverse field distribution.
17. T. A. Birks, P. S. J. Russell, and D. O. Culverhouse, "The acousto-optic effect in single-mode fiber tapers and couplers," J. Lightwave Technol. **14**, 2519–2529 (1996).
18. A. Yariv and P. Yeh, *Photonics: Optical Electronics in Modern Communications*, 6th ed. (Oxford University Press, USA, 2007).
19. S. E. Harris, J. E. Field, and A. Imamoğlu, "Nonlinear optical processes using electromagnetically induced transparency," Phys. Rev. Lett. **64**, 1107–1110 (1990).
20. K.-J. Boller, A. Imamoğlu, and S. E. Harris, "Observation of electromagnetically induced transparency," Phys. Rev. Lett. **66**, 2593–2596 (1991).
21. M. Fleischhauer, A. Imamoglu, and J. P. Marangos, "Electromagnetically induced transparency: Optics in coherent media," Rev. Mod. Phys. **77**, 633–673 (2005).
22. Although our scheme is closer to the ladder-type configuration considering the order of the propagation constants, we relate the current scheme to the lambda-type configuration to avoid unnecessary confusion. Whereas the dark state in a ladder-type atomic configuration is not strictly stable, our implementation does not contain decaying processes and therefore has a steady dark state leading to an efficient induced transparency.
23. P. M. Anisimov, J. P. Dowling, and B. C. Sanders, "Objectively discerning Autler-Townes splitting from electromagnetically induced transparency," Phys. Rev. Lett. **107**, 163604 (2011).
24. M. Neeley, M. Ansmann, R. C. Bialczak, M. Hofheinz, E. Lucero, A. D. O'Connel, D. Sank, H. Wang, J. Wenner, A. N. Cleland, M. R. Geller, and J. M. Martinis, "Emulation of a quantum spin with a superconducting phase qubit," Science **325**, 722–725 (2009).
25. The retained maximum transmission (83%) and the voltage (9.5 V_{pp}) of the next minimum transmission, however, deviate from 100% and 2×4 V_{pp}, respectively. These discrepancies arise mainly from an off-resonant coupling due to non-uniformity of the fibre and also from the saturation of the acoustic transducer efficiency.
26. S. H. Autler and C. H. Townes, "Stark effect in rapidly varying fields," Phys. Rev. **100**, 703–722 (1955).
27. H. E. Engan, B. Y. Kim, J. N. Blake, and H. J. Shaw, "Propagation and optical interaction of guided acoustic waves in two-mode optical fibers," J. Lightwave Technol. **6**, 428–436 (1998).
28. P. Kwiat, H. Weinfurter, T. Herzog, and A. Zeilinger, "Interaction-free measurement," Phys. Rev. Lett. **74**, 4763–4766 (1995).

1. Introduction

State transfer by coherent coupling is a key element of many optical devices as well as various quantum mechanical phenomena. Analogies between optical interference and temporal evolution of coupled quantum states have led to designing novel photonic waveguide devices inspired by coherent quantum effects in atomic or molecular physics [1, 2]. For example, optical analogues to a multi-level atom have reproduced electromagnetically induced transparency (EIT) [3–7], stimulated Raman adiabatic passage [8–11], and quantum Zeno effect [12], resulting in novel photonic devices. These examples controlled the coupling strength and the selection rule solely by the proximity and/or the phase matching between the optical modes, unlike the original atomic level configuration whose coupling is controlled by external driving fields. This work realizes external resonant couplings between the spatial modes of a few-mode fiber (FMF) by flexural acoustic waves propagating along the fiber. The symmetry of the transverse mode profiles determines the allowed or forbidden couplings between the spatial modes, as the selection rule of the dipole transition between the atomic states. Narrow-bandwidth transmission analogous to EIT and Autler-Townes splitting (ATS) is experimentally demonstrated. To our knowledge, this is the first demonstration of acousto-optic (AO) three-mode coherent coupling as well as the first implementation of an optical analogue to a three-level atom with resonant coupling fields. The demonstrated structure is an efficient mode converter that is applicable to space-division multiplexing (SDM) communications [13, 14]. For example, one can implement an arbitrarily mode-selectable router to a multi-mode fiber transmission line when combined with a multi-mode fiber directional coupler that couples the same spatial modes of two fibers.

#202694 - $15.00 USD Received 6 Dec 2013; revised 10 Jan 2014; accepted 12 Jan 2014; published 23 Jan 2014

2. Device structure and operation principle

The fiber in this work has a step-index elliptic-core (numerical aperture 0.16, core diameter 11 μm $\times$ 7 μm) with a cladding diameter 100 μm. Around the wavelength of 1550 nm, the fiber guides in its core two spatial modes, the fundamental LP_{01} mode and the 'even' LP_{11} mode whose intensity lobes are aligned along the major axis of the core. The 'odd' LP_{11} mode is cut off from the core [15]. The third mode is the LP_{03} mode, which is a 'cladding mode' that is guided not by the core-cladding boundary but by the cladding-air boundary of an unjacketed fiber section. Advantage of using the LP_{03} mode among available modes is that the refractive index difference between the LP_{11} and the LP_{03} modes is close to the difference between the LP_{01} and the LP_{11} modes in the given fiber such that the required driving frequencies for both transitions lie in the effective bandwidth of our acoustic transducer.

A piezoelectrically driven acoustic transducer generates two flexural acoustic waves of different frequencies along the fiber as shown in Fig. 1(a). The flexural acoustic waves introduce antisymmetric perturbation to the optical path length throughout the fiber cross section, thus the symmetric LP_{0i} modes can be coupled to the antisymmetric LP_{1j} modes, and the antisymmetric LP_{1j} modes can be coupled to the doubly antisymmetric LP_{2k} or the symmetric LP_{0l} modes $(i, j, k, l = 1, 2, 3, ...)$ [16, 17]. Coherent mode conversion occurs when the acoustic wavelength matches the intermodal beat length $\lambda/|n_1 - n_2|$, where λ is the optical wavelength and n_1, n_2 are effective refractive indices of the two modes, respectively. Propagation of each mode under the influence of the AO coupling is described by the following coupled mode equations [18]:

$$\begin{aligned} \frac{dA_{01}}{dz} &= i\kappa_p A_{11} e^{-2i\delta_p z}, \\ \frac{dA_{11}}{dz} &= i\kappa_p^* A_{01} e^{2i\delta_p z} + i\kappa_c A_{03} e^{-2i\delta_c z}, \\ \frac{dA_{03}}{dz} &= i\kappa_c^* A_{11} e^{2i\delta_c z}, \end{aligned} \tag{1}$$

where z is the propagation distance along the fiber, A_{01}, A_{11}, and A_{03} are respectively the field amplitudes of the three modes, κ_p (κ_c) is the coupling coefficient between modes LP_{01} and LP_{11} (LP_{11} and LP_{03}), and δ_p (δ_c) is the phase mismatch of the coupling $\delta_p = \pi(n_{01} - n_{11})/\lambda \pm \pi/\Lambda_p$ ($\delta_c = \pi(n_{11} - n_{03})/\lambda \pm \pi/\Lambda_c$), where $\Lambda_{p,c}$ is the acoustic wavelength. The above equations are equivalent to the master equation for the lambda-type laser-driven atomic states with no dephasing or decaying terms for pure initial states [19–22]. Temporal evolution of the atomic state is replaced by spatial propagation of the light along the fiber. This equivalence is illustrated in Fig. 1(b). Each spatial mode corresponds to one energy level of the lambda-type configuration, and different phase velocities play a role of different energies between the states. AO coupling coefficients κ's are equivalent to the Rabi frequencies by the external driving fields in the lambda scheme. As our system has no decaying terms, in a strict sense [23] the configuration is in the ATS regime rather than in the EIT regime.

Figure 1(c) shows the far field patterns of the spatial modes measured with cleaving the end part of the unjacketed AO interaction region. To generate the LP_{11} mode and the LP_{03} mode from the initial LP_{01} mode, acoustic amplitudes are set as $\kappa_p = \kappa_0$, $\kappa_c = 0$ and $\kappa_p \cong \kappa_c \cong \sqrt{2}\kappa_0$, respectively, where $\kappa_0 = \pi/(2L)$ with L being the AO interaction length. Here two identical coupling efficiencies enable complete transfer to the LP_{03} mode. This can also be interpreted as an analogy to the spin-1 rotation of a qutrit [24].

3. Experimental results and discussions

For characterization of the induced transparency, the LP_{01} mode enters the FMF from a lead single-mode fiber, and, after the AO interaction region, a mode stripper (MS) that is a tightly

#202694 - $15.00 USD Received 6 Dec 2013; revised 10 Jan 2014; accepted 12 Jan 2014; published 23 Jan 2014

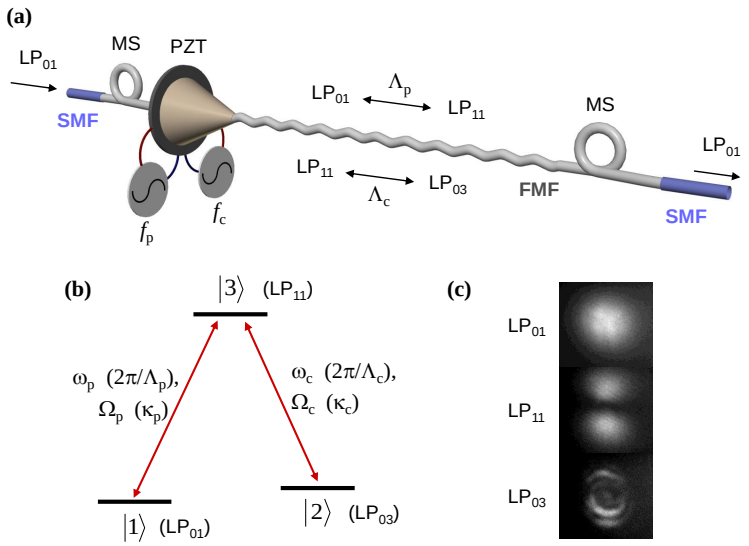

Fig. 1. Experimental scheme. (a) Structure of the acoustooptic three-mode coupler. (b) Equivalent lambda-type atomic state configuration. Labels in the parentheses denote corresponding parameters in our scheme. (c) Measured far field patterns of the spatial modes. ω_p (ω_c): the electromagnetic frequency of the probe (coupling) field, Ω_p (Ω_c): the Rabi frequency by the probe (coupling) field, f_p (f_c): the probe (coupling) acoustic frequency, Λ_p (Λ_c): the probe (coupling) acoustic wavelength, κ_p (κ_c): the coupling coefficient by the probe (coupling) acoustic wave. FMF: few-mode fiber, SMF: single-mode fiber, MS: mode stripper, PZT: piezoelectric transducer.

bound fiber section removes the more weakly guided LP_{11} mode while preserving the LP_{01} mode. The efficiency of the mode removal is $\geq 99\%$. The LP_{03} mode is removed by the fiber jacket just after the AO interaction. The AO interaction length L is 50 cm. The probe acoustic frequency f_p for the LP_{01}-LP_{11} conversion is 3.733 MHz with the corresponding acoustic wavelength Λ_p of 436.3 μm. The conversion efficiency is set as 100% by adjusting the coupling coefficient $\kappa_c = \pi/(2L)$. The FMF has been designed to match the group velocities of the LP_{01} mode and the LP_{11} mode around the wavelength of 1580 nm [15]. Therefore the phase matching for the LP_{01}-LP_{11} conversion is preserved in the first order of the wavelength difference, and the transmission spectrum shows a broad-bandwidth notch as shown in Fig. 2(a).

The coupling acoustic frequency f_c (wavelength Λ_c) for the LP_{11}-LP_{03} conversion is 2.883 MHz (505.0 μm). The transmission spectrum while applying the coupling acoustic wave with the coupling coefficient $\kappa_c = 3\kappa_0$ is shown in Fig. 2(b). The transparency induced by the LP_{11}-LP_{03} coupling shows a narrow half-maximum bandwidth (2 nm) due to a non-zero group index difference between the LP_{11} and LP_{03} modes, which is estimated to be 0.005. The small side lobes of the transmission peak are attributed to the nonuniformity of the fiber geometry along the interaction length.

The magnitude of the peak transmission is measured while varying the two coupling coefficients as shown in Figs. 3(a) and 3(b). The transmission due only to the LP_{01}-LP_{11} probe field is shown in Fig. 3(a). Maximum mode conversion occurs at the applied voltage of 4 V_{pp} with reaching the minimum transmission of 0.9%, and the higher voltage range shows the overcoupling behavior [25]. The magnitude of the induced transparency by the coupling field is

#202694 - $15.00 USD Received 6 Dec 2013; revised 10 Jan 2014; accepted 12 Jan 2014; published 23 Jan 2014

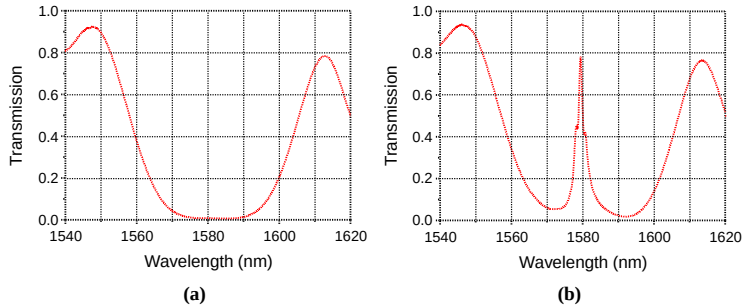

Fig. 2. Transmission spectra of the LP_{01} mode: (a) with only the probe acoustic wave that makes 100% coupling between the LP_{01} mode and the LP_{01} mode ($\kappa_p = \kappa_0 = 2\pi/L$). (b) with the coupling wave additionally applied between the LP_{11} mode and the LP_{03} mode ($\kappa_c \cong 3\kappa_0$).

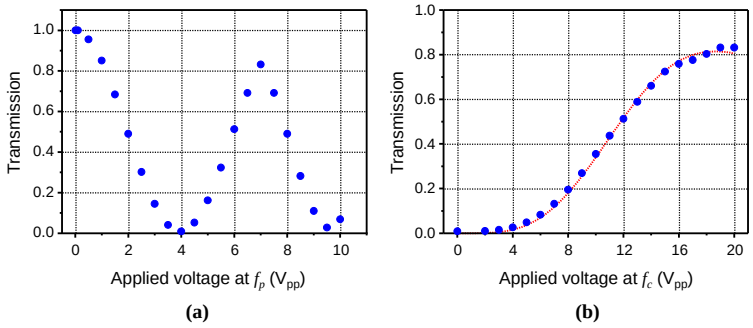

Fig. 3. Transmission of the LP_{01} mode at the center wavelength: (a) when only the probe acoustic wave is applied, and (b) when the coupling acoustic wave is applied with the probe amplitude fixed at the voltage of 4 V_{pp}. The solid line is the fitting result based on Eq. (2).

shown in Fig. 3(b) with the theoretical fit based on the solution of Eq. (1) expressed as

$$T = \frac{|\kappa_c|^2 + |\kappa_p|^2 \cos\left(\sqrt{|\kappa_p|^2 + |\kappa_c|^2}\, z\right)}{|\kappa_p|^2 + |\kappa_c|^2}. \tag{2}$$

A constant 0.814 is multiplied to Eq. (2) as an attenuation factor, and the fitted voltage for $\kappa_c = \kappa_0$ is 4.81 V.

To more clearly reveal the coherent nature of the induced transparency, the transparency is undone by detuning the probe field. In a dressed state picture, the coupling field in Fig. 1(b) converts the state $|3\rangle$ into two superposed states whose energy levels are higher or lower than that of $|3\rangle$ by the Rabi frequency Ω, respectively, between $|2\rangle$ and $|3\rangle$. Therefore detuning the probe frequency by $\pm\Omega$ retains the coherent absorption from $|1\rangle$ [3, 26]. The current system realizes this Autler-Townes effect by shifting the acoustic propagation constant $2\pi/\Lambda_p$ by κ_c. Transmission of the LP_{01} mode while tuning the acoustic frequency is shown in Fig. 4(a). κ_c is fixed as in Fig. 2(b) ($\kappa_c \cong 3\kappa_0$). Two notches appear on both sides of the central transmission peak with the separation $2\Delta f_p = 8$ kHz.

The detuning for each notch is compared with the magnitude of the applied coupling field. According to the acoustic dispersion relation [27], the frequency shift leads to the change of the acoustic propagation constant $\Delta(2\pi/\Lambda) = -2\pi/\Lambda^2(d\Lambda_p/df_p)\Delta f_p$ of 8.9 m^{-1} because

#202694 - $15.00 USD Received 6 Dec 2013; revised 10 Jan 2014; accepted 12 Jan 2014; published 23 Jan 2014

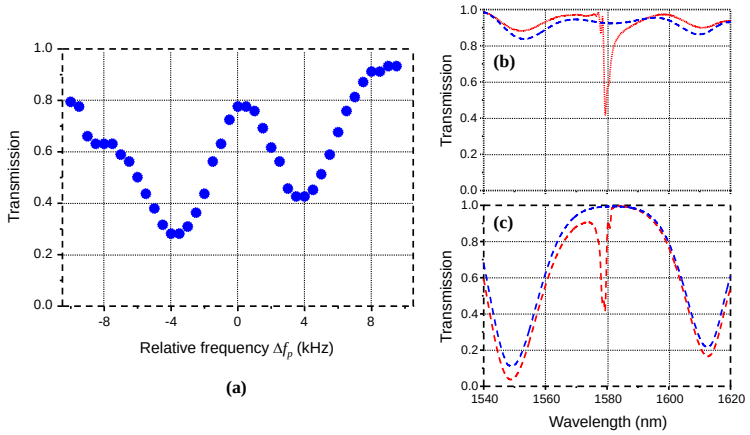

Fig. 4. Induced absorption of the LP_{01} mode with the probe frequency f_p detuned by Δf_p: (a) transmission at the center wavelength, (b) transmission spectrum for $\Delta f_p = +4$ kHz, and (c) transmission spectrum for $\Delta f_p = -4$ kHz. Dashed lines denote the spectra with the coupling acoustic wave turned off.

$d\Lambda_p/df_p = -0.067$ μm/kHz. As $\kappa_0 = \pi/(2\times 0.5\text{ m}) = \pi$ m^{-1}, $\Delta(2\pi/\Lambda)$ equals to $2.8\kappa_0$ and agrees with the coupling coefficient κ_c verified in Figs. 2 and 3. The difference of the two notch depths in Fig. 4(a) is due to the frequency dependence of the acoustic transducer. Figures 4(b) and 4(c) show the transmission spectra for $\Delta f_p = +4$ kHz and $\Delta f_p = -4$ kHz, respectively, with the coupling field turned on (solid lines) and off (dashed lines). The induced absorption notches are clearly seen in the spectra when the coupling field is turned on. The two broad notches in Fig. 4(c) by the LP_{01}-LP_{11} conversion verify that the modal beat length is the maximum at 1580 nm and decreases at both higher and lower wavelengths.

The presented scheme can be extended to more than three modes. Generally an LP_{lm} mode can be coupled to an $LP_{(l-1)m'}$ mode or an $LP_{(l+1)m'}$ mode ($m, m' = 1, 2, 3, \cdots$) considering the symmetry of the mode profiles and the acoustic perturbation to the local refractive index [17]. Coupling between two core modes is generally more efficient than between a core mode and a cladding mode because of a greater mode overlap. Therefore a fiber that guides a greater number of core modes will be useful for realizing a more complex level configuration. Moreover, a lower-NA fiber is generally desirable because the required acoustic frequencies are lower, and accordingly the acoustic amplitudes are higher for a fixed input power of the acoustic transducer.

4. Conclusions

In conclusion, AO three-mode coupling in an optical fiber has been successfully demonstrated. AO conversion from the fundamental LP_{01} mode to the LP_{03} mode has been demonstrated for the first time to our knowledge. As an analogy to EIT in a lambda-type atom, transmission of the LP_{01} mode has been induced by the coupling between the LP_{11} mode and the LP_{03} mode. This three-level coupling can also be conceptually compared to the interaction-free measurement [28], whose repeated interrogation of interferometers is replaced by continuous coherent coupling between the copropagating modes. The presented scheme can be extended to visualize the coherent nature of a multi-level atomic structure, and inspire the development of novel devices that perform unique functions for multiplexing and demultiplexing the spatial modes in future communication systems.

#202694 - $15.00 USD Received 6 Dec 2013; revised 10 Jan 2014; accepted 12 Jan 2014; published 23 Jan 2014

Acknowledgments

This work has been supported by the KRISS project 'Convergent Science and Technology for Measurements at the Nanoscale.' The authors thank K. J. Park and Prof. B. Y. Kim in KAIST for help with the experimental setup.

#202694 - $15.00 USD Received 6 Dec 2013; revised 10 Jan 2014; accepted 12 Jan 2014; published 23 Jan 2014